HAL open science

Vaporization characteristics of an isolated ethanol droplet at flame conditions

Deniz Kaya Eyice, Guillaume Renoux, Fabien Halter, Ahmet Yozgatlıgil, İskender Gökalp, Christian Chauveau

To cite this version:

Deniz Kaya Eyice, Guillaume Renoux, Fabien Halter, Ahmet Yozgatlıgil, İskender Gökalp, et al.. Vaporization characteristics of an isolated ethanol droplet at flame conditions. Atomization and Sprays, 2022, 32 (9), pp.79-94. 10.1615/AtomizSpr.2022041118 . hal-03725375

HAL Id: hal-03725375

https://hal.science/hal-03725375v1

Submitted on 17 Oct 2022

HAL is a multi-disciplinary open access archive for the deposit and dissemination of scientific research documents, whether they are published or not. The documents may come from teaching and research institutions in France or abroad, or from public or private research centers.

L'archive ouverte pluridisciplinaire **HAL**, est destinée au dépôt et à la diffusion de documents scientifiques de niveau recherche, publiés ou non, émanant des établissements d'enseignement et de recherche français ou étrangers, des laboratoires publics ou privés.

VAPORIZATION CHARACTERISTICS OF AN ISOLATED ETHANOL DROPLET AT FLAME CONDITIONS

Deniz Kaya,[1,2,3,*] Guillaume Renoux,[1,2] Fabien Halter,[1,2] Ahmet Yozgatlıgil,[3] İskender Gökalp,[1,3] & Christian Chauveau[1]

[1]*CNRS-INSIS, Institut de Combustion, Aérothermique, Réactivité et Environnement, Orléans, 45071, France*

[2]*Université d'Orléans, Orléans, 45100, France*

[3]*Department of Mechanical Engineering, Middle East Technical University, Ankara, 06800, Turkey*

*Address all correspondence to: Deniz Kaya, CNRS-INSIS, Institut de Combustion, Aérothermique, Réactivité et Environnement, 1C Avenue de la Recherche Scientifique, Orléans, 45071, France, E-mail: deniz.kaya@cnrs-orleans.fr

Original Manuscript Submitted: mm/dd/yyyy; Final Draft Received: mm/dd/yyyy

The aim of this study is to investigate single ethanol droplet evaporation characteristics under premixed CH_4/air flame conditions via experimental and numerical approaches. In the experimental part of the study, ethanol droplet with an initial diameter between 20 and 70 μm was injected through a flat laminar stagnant flame. Visualization of the flame front and temporal monitoring of the droplet evaporation at high temperatures up to 2200 K were performed using planar laser tomography. Droplet motion and its diameter change are captured simultaneously via PIV/PTV and ILIDS diagnostics, respectively. Velocity measurements indicated that the droplets are small enough to be carried by surrounding gas with a very small slip velocity. Variation in droplet diameter is successfully tracked through the flame via ILIDS and it is found to be more drastic in burnt gases. Hence, vaporization rates are reported at burnt gas temperature which is affected by the heat losses from flame to the stagnation plate due to the change in the temperature profile. In the numerical part of the study, single droplet evaporation under constant temperature and stagnant environment was studied with Spalding model using YALES2 solver. The variations of the droplet properties were computed under N_2 atmosphere and under flame conditions. At elevated conditions, flame temperature is found to have a more dominant effect on the evaporation rate rather than the burnt gas composition.

1. INTRODUCTION

Spray combustion is a complex phenomenon involving many processes; atomization, droplet vaporization, mixing, turbulence, chemical kinetics, as well as the interaction of these processes. In industrial applications, high rates of evaporation and mixing of liquid fuel with the gas phase are desired for high energy efficiency. Several droplet-droplet, droplet-turbulence and droplet-flame interactions are observed in real-life applications. Among all situations occurring in combustion chambers, one of the basic processes is the interaction of a single droplet with a flamelet that is being laminar and locally 1D structures of the flame (Driscoll, 2008; Peters, 1984). It is reported in many studies that droplets are causing structural changes on flame front while altering the local flame properties (Lawes et al., 2006; Nassouri et al., 2013; Renoux et al., 2018; Thimothée et al., 2016). Hence, it is essential to investigate whether the droplet can reach to flame zone by identifying the evaporation characteristics and then, it will be useful to understand the local changes in flamelet caused by droplets.

The characterization of droplet behavior yields a great importance in order to classify the combustion regime. The droplets may evaporate in the reaction zone resulting in single-phase combustion. Whereas, some droplets may cross the flame front, may or may not burn beyond it which may cause local changes in the flame structure (Mercier et al., 2007; Orain and Hardalupas, 2014; Verdier et al., 2018) and flame instabilities (Renoux et al., 2018; Thimothée et al., 2017). Subsequently, the prediction of the droplet lifetime becomes highly important for design considerations. Several experimental studies have been performed under different ambient conditions in order to determine the characteristic evaporation time for a variety of fuels including ethanol (Muelas et al., 2020; Saharin et al., 2012; Yozgatligil et al., 2004), kerosene (Ghassemi et al., 2006), n-heptane and several other long chain paraffins (Chauveau et al., 2019; Gokalp et al., 1994; Muelas et al., 2020; Verwey and Birouk, 2018) with their blends (Chen et al., 1997; Keller et al., 2015; Maqua et al., 2008). For the majority of reported studies, the evaporation rate measurements have been performed under stagnant ambient at constant temperature varying from 400 K up to 1000 K. However, for a droplet moving in the flame field, it will encounter

a steep temperature profile varying between 300-2200 K and it will be surrounded by a non-stationary gas mixture. Hence, it is important to analyze how low temperature evaporation rates correlate with the ones measured at high temperatures which will be reported in the scope of this study.

Single droplet evaporation has been studied also numerically in order to improve and validate proposed models under several ambient temperature, pressure and fuel vapor concentration. Ethanol has been selected because of the availability of reliable experimental data, water condensation effects and its blends with other fuels to study multicomponent models (Al Qubeissi et al., 2018; Millán-Merino et al., 2021; Narasu et al., 2020; Ni et al., 2021; Pinheiro et al., 2019). Al Qubeissi et al. studied the effect of ambient conditions under 400-650 K at a wide range of pressure considering radiative effects (Al Qubeissi et al., 2018). They reported that droplet lifetime decreases under elevated conditions for a variety of ethanol/gasoline mixture as well as pure ethanol at temperatures greater than 400 K. Narasu and co-workers studied ethanol/water bicomponent droplet evaporation under dry and humid convective air with Abramzon-Sirignano model (Abramzon and Sirignano, 1989) introducing non-ideal mixture consideration (Narasu et al., 2020). They concluded that the evaporation behavior of bicomponent droplet is different under dry and humid conditions because of the fact that water from the ambient is condensed to droplet and this situation delays its vaporization. As it is reported in the literature, the ambient conditions have an influence on evaporation characteristics and the behavior may change depending on the ambient temperature and pressure.

In this study, the evaporation of an isolated ethanol droplet through a CH_4/air premixed flame is studied both experimentally and numerically. The diameter and velocity of the droplet are measured at each 25 μs while it is interacting with a laminar premixed stagnation flame under lean, stoichiometric and rich conditions. Hence, the evaporation rate of ethanol at elevated temperatures is reported and its dependency to initial droplet diameter and flame temperature is investigated experimentally which has never been studied in the literature to the authors knowledge. The simulations are performed with Spalding model under stagnant N_2 atmosphere and burnt gas conditions at constant temperature for a stationary droplet in order to report the effect

of gas phase concentration to the evaporation rate.

2. EXPERIMENTAL

2.1 Flat flame burner

In this study, a flat flame burner is used to observe the droplet evaporation sequence through a stationary premixed laminar flame. A N_2 co-flow is used to facilitate flame stabilization. Premixed mixture of air and fuel passes through a laminarization grid and then is accelerated by a converging section. The mixture is ignited with an external igniter at the region between stagnation plate and the burner outlet. With a continuous premixed mixture feeding, a laminar and flat flame is created at the specified conditions and it is stabilized thanks to the presence of an upper stagnation plate located 25 mm away from the burner outlet. Monodispersed liquid ethanol droplets with 50 μm diameter are generated by a piezoelectric injector (Microdrop Technologies MD-K-140). The frequency of the droplet injection is adjusted accordingly to provide enough time between droplet injections and to avoid coagulation and close-distance droplets. The droplets are carried by premixed gas flow in a needle having an internal diameter of 3 mm up to the main flow by drag. The residence time of the droplets in needle is nearly 500 ms leading to small changes of the droplet diameter at the exit of the burner plate. Droplets are then, fed to the flame zone perpendicularly from the centerline of the burner. The schematic of flat flame burner is given in Fig. 1.a. Details of the flat flame burner can also be found in other studies (Renoux (2020); Thiesset et al. (2017)).

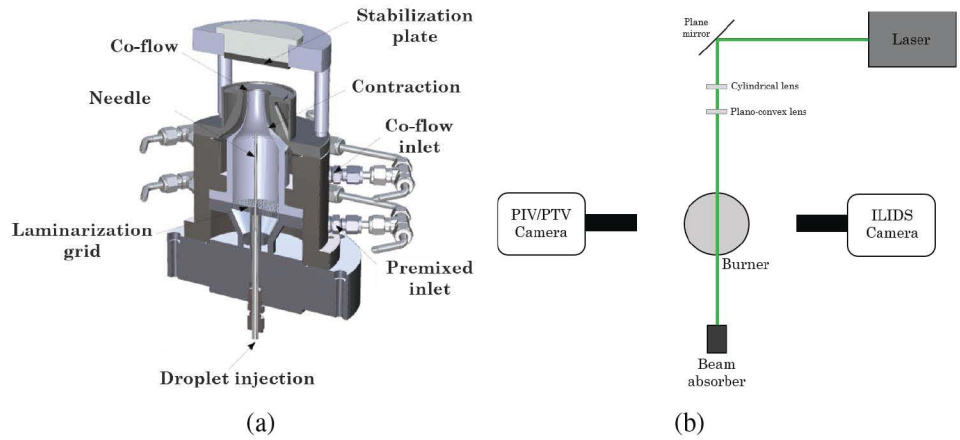

FIG. 1: (a) Schematic of the flat flame burner (Thiesset et al., 2017) (b) Experimental configuration

Experimental configuration is represented in Fig. 1.b. The burner is coupled with a laser device, Coherent Verdi emitting at 532 nm and 2D laser sheet is created from a continuous laser beam with the help of one semi-cylindrical divergent lens (f_2 = -25 mm) and one plano-convex lens (f_2 = 500 mm). Two high-speed cameras, Phantom v1210 and Phantom v1611 both equipped with Sigma APO Macro 180 mm lens at maximum opening are placed perpendicularly to the flame in order to observe the scattered light. The first one is dedicated to velocity measurements by PIV (Particle Image Velocimetry) and PTV (Particle Tracking Velocimetry), while the second one will be dedicated to drop size determination by ILIDS (Interferometric Laser Imaging for Droplet Sizing) measurement. For PIV/PTV camera, 22.9 μm/pixel resolution is obtained.

2.2 Planar laser tomography techniques and postprocessing

Visualization of the flame front and temporal monitoring of the droplet evaporation are performed using planar laser tomography. Mie scattering is utilized to determine the position of the flame front and the velocity of unburnt gases via Particle Image Velocimetry (PIV). Seeding of the premixed gas is achieved through the dispersion of diethylhexyl-sebacate (DEHS) droplets with a size of approximately 2-4 μm in diameter. The flame contour is identified using a threshold technique. The location of the flame front is determined at T=525 K isotherm where DEHS droplets evaporate, given in Fig.2 as a green line. In order to measure the velocity of the unburnt

gases, an open-source MATLAB library PIVlab is used (Thielicke and Stamhuis, 2014). By comparing two successive images and calculating the displacement of DEHS droplets between two images, the local displacement of the unburnt gas is determined. The main assumption of this method is that DEHS droplets are small enough to follow the gas flow. Velocity vectors of unburnt gases are given in Fig. 2.a.

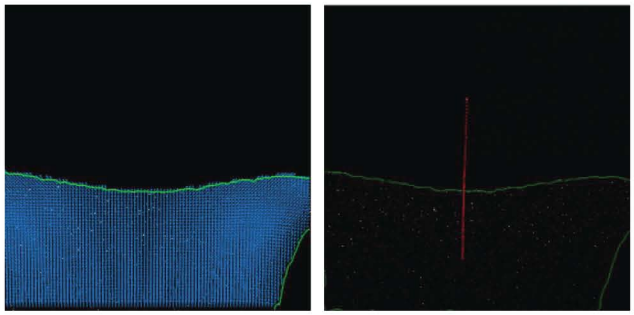

(a) (b)

FIG. 2: (a) Determination of the flame front and the velocity of unburnt gases based on PIV (b) Trajectory of the droplet based on PTV (d_0 = 35 μm)

The motion of the droplet is also determined via Mie scattering using Particle Tracking Velocimetry (PTV). Initial position of the droplet is determined from the first image of the sequence based on the largest connected luminous pixels to initiate Kanade-Lucas-Tomasi (KLT) algorithm. For each subsequent frame, the location of the ethanol droplet is tracked with KLT feature tracking algorithm in MATLAB Computer Vision library. Thereupon, the displacement speed of the droplet in the reference of the laboratory is calculated. The tracked droplet trajectory is represented in Fig. 2.b.

In addition, Interferometric Laser Imaging for Droplet Sizing (ILIDS) is coupled with Mie scattering to obtain the droplet size variation during evaporation. The high-speed camera used for ILIDS allows obtaining a good temporal resolution for the evolution of the droplet size by defocusing and capturing the interference fringe pattern of the droplet at each frame. By providing a high laser power, it is possible to increase the detection of fringes even the droplet size is very small due to fact that ILIDS method is based on the reflected and the refracted rays visible on the droplet surface. In this study, 20 Watts laser power is used which is enough to detect 2-3 fringes at the last image recorded for ethanol droplet. The number of fringes is

computed for an individual droplet at each frame based on Discrete Fourier Transform (DFT) on the five vertical sections of the fringe pattern. With the help of peak intensities in Fourier space, the fringes are detected and computed. Fringe patterns for a droplet from consecutive frames while passing through the flame is illustrated in Fig. 3.

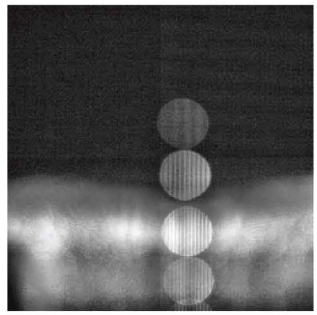

FIG. 3: Combined sequence of ILIDS images illustrating the evaporation of a droplet while passing through the flame front (droplet diameters from bottom to top; 49 μm, 49 μm, 38 μm and 15 μm)

The droplet diameter based on the number of fringes is then calculated from the following relation (Renoux et al., 2018);

$$d = N_{fringe}\frac{2\lambda}{\alpha}\left[cos(\theta/2) + \frac{m\,sin(\theta/2)}{\sqrt{m^2 - 2\,m\,cos(\theta/2) + 1}}\right]^{-1} \tag{1}$$

where d is the particle diameter, N_{fringe} is the number of fringes on the droplet, θ is the scattering angle (here, 90°), α is the collecting angle, λ is the laser wavelength (here, 532 nm) and m is the refractive index of the droplet. In this configuration, 3.52 μm/fringe resolution is obtained.

The cameras for PIV/PTV and ILIDS have different acquisition frequencies, 10,000 and 40,000 images per second, respectively. In order to have the same time reference, the camera acquisition sequence is triggered by a common trigger signal. They are then synchronized in time in order to combine different diagnostics. Experiments are performed with ethanol droplet as the liquid fuel and CH_4/air premixed flames at ϕ=0.8, 0.9, 1.0 and 1.1 which are reported based on gaseous CH_4/air flame. For each sequence of experiments, individual droplets are selected over all recordings and the complete postprocessing is performed for each individual droplet in order

to track its evaporation.

3. NUMERICAL

Computations are performed with YALES2 solver, based on the finite volume method for low Mach number flows with variable density (Moureau et al., 2011). Eulerian-Lagrangian (EL) approach is used to model the two-phase flow in which a droplet is considered as an isolated point in Lagrangian frame, while the gas phase is represented with the Eulerian description. Two-way coupling approach is utilized in order to transfer mass, momentum and energy from the liquid phase to the gas phase via source terms.

3.1 Evaporation model

The evaporation of the droplet is computed using Spalding model (Spalding, 1950). In this model, droplets are assumed to be spherical, isolated, mono-component, having infinite thermal conductivity and uniform temperature. The surface of the droplet is assumed to be in thermo-dynamic equilibrium with the surrounding gas. Droplet mass temporal evolution is determined assuming the fuel mass flux leaving the droplet surface equal to the variation of mass of the droplet;

$$\frac{dm_p}{dt} = \dot{m}_p = -\pi\, d\, Sh\, \rho_p\, \mathcal{D}\, ln(1 + B_M) \tag{2}$$

where Sh is the Sherwood number, ρ_p is the density of the particle, $\mathcal{D}$ is the diffusion coefficient and B_M is Spalding mass number defined as;

$$B_M = \frac{Y_s - Y_\infty}{1 - Y_s} \tag{3}$$

where Y_s is the evaporated mass fraction of the droplet at the surface estimated by Clasius-Clapeyron relation using the partial saturated vapor pressure at the surface of the droplet;

$$P_s = P_{ref} \left[\frac{W\, L_v}{R} \left(\frac{1}{T_{evap}} - \frac{1}{T_p} \right) \right] \tag{4}$$

where W is the molar mass and L_v is the latent heat of vaporization. T_{evap} is the evaporation temperature of the droplet at the reference pressure, P_{ref}=1 atm. Y_∞ is the evaporated mass fraction at the far field whose properties are computed by 1/3 rule (Hubbard et al., 1975). Using the relation of mass variation, the change in droplet diameter is expressed as;

$$d^2 = d_0^2 - \frac{8\,\rho_g\,\mathcal{D}}{\rho_p} ln(1 + B_M)t = d_0^2 - K\,t \tag{5}$$

where d_0 is the initial diameter of the droplet, ρ_g is the density of gas and t is the time. Eq. (5) is also known as d^2 law at which the rate of evaporation, K can directly be obtained.

The temporal evolution of the droplet temperature is estimated by integrating the energy conservation equation from the surface of the droplet to the far field;

$$\frac{dT_p}{dt} = \frac{\dot{m_p}}{m_p\,C_p}\left[\frac{C_{p,ref}}{B_T}(T_s - T_\infty) + L_v\right] \tag{6}$$

where C_p is the specific heat of the droplet and B_T is the Spalding heat number defined as;

$$B_T = (1 - B_M)^{\frac{Sh\,Pr}{Nu\,Sc}} - 1 \tag{7}$$

where Pr is the Prandtl number, Sc is the Schmidt number. Sh and Nu are the Sherwood and Nusselt numbers, respectively and they are taken as constant since there is no convection taken into account around the droplet. Particle Reynolds number, Re_p is also defined as;

$$Re_p = \frac{d\,|u_p - u_\infty|}{\nu} \tag{8}$$

where ν is the kinematic viscosity.

For evaporation computations, an isolated ethanol droplet having 50 μm initial diameter is injected at T=300 K and P=1 atm at the center of a large Cartesian cube with dimensions $10 \times 10 \times 10$ cm^3 to avoid edge effects. Evaporation of the droplet is tracked until complete evaporation at constant temperature and stagnant ambient with pure N_2 (373-2250 K) and burnt gases (1800-2200 K). Burnt gas compositions are computed in Cantera for CH_4/air flames at

equivalence ratios ranging between 0.8-1.1 with different kinetic mechanisms. Droplet diameter, droplet temperature and Spalding numbers are computed during evaporation process.

3.2 Flame field computations

Laminar flame computations are performed in Cantera (Goodwin et al., 2018) using COFFEE mechanism with 14 species and 39 reactions (Coffee, 1984) and detailed San Diego mechanism with 57 species and 268 reactions (University of California San Diego, Mechanical and Aerospace Engineering-Combustion Research, 2016). 1D freely propagating adiabatic flame field is computed using multispecies transport for CH_4/air (21% O_2+79% N_2) mixtures having different equivalence ratios (ϕ=0.8, 0.9, 1.0, 1.1) at 1 atm and 300 K. The domain length is set to 25 mm which is the distance between burner exit and stagnation plate in experimental configuration. The grid parameters are adjusted gradually in order to obtain a converged solution.

1D stagnation flame field is also computed using multispecies transport at the same flame conditions in order to understand the effect of heat exchange between flame and stagnation plate on evaporation as well as to obtain a more realistic configuration. The inlet velocity of the fresh gases, u_0 are computed based on the mass flow rates fed to the system in the experimental configuration. Since the experimental measurement of the stagnation plate temperature is not performed, first, the sensitivity of the flame temperature to the plate temperature is studied. It is seen that for the plate temperature ranging between 500-1500 K, the flame temperature is changing nearly by ± 10 K. Due to the fact that the injected droplets are evaporating in the burnt gases and they cannot reach near to the plate, the plate temperature is assumed to be constant at 500 K.

Computed laminar flame speeds, S_L^0 and burnt gas temperatures, T_b are given in Table 1 below for all experimental conditions. It can be seen that the burnt gases temperature is slightly lower in the stagnant flame configuration due to the heat loss though the stagnation plate.

TABLE 1: Calculated flame parameters with COFFEE scheme

ϕ	Adiabatic flame		Stagnation flame		
	S_L^0 *(m/s)*	T_b *(K)*	U_0 *(m/s)*	S_L^0 *(m/s)*	T_b *(K)*
0.8	0.320	1993.7	0.560	0.341	1982.9
0.9	0.383	2120.7	0.743	0.409	2105.6
1.0	0.423	2202.5	0.824	0.451	2188.0
1.1	0.434	2200.5	0.699	0.453	2191.4

Since Rayleigh scattering signal is completely shadowed by Mie scattering signal, the temperature of the gas field cannot be obtained experimentally during PIV/PTV measurements. Instead, 1D temperature profiles of computed adiabatic and stagnation flames with COFFEE scheme is fitted to the corresponding experimental field, given in Fig. 4. From PIV results, the position of the flame front is determined based on the presence of DEHS droplets. By taking the isotherm T=525 K being the evaporation temperature of DEHS droplets, calculated temperature profiles, thermodynamic and transport properties are fitted to the experimental flame field in order to track the droplet evaporation through flame front experimentally.

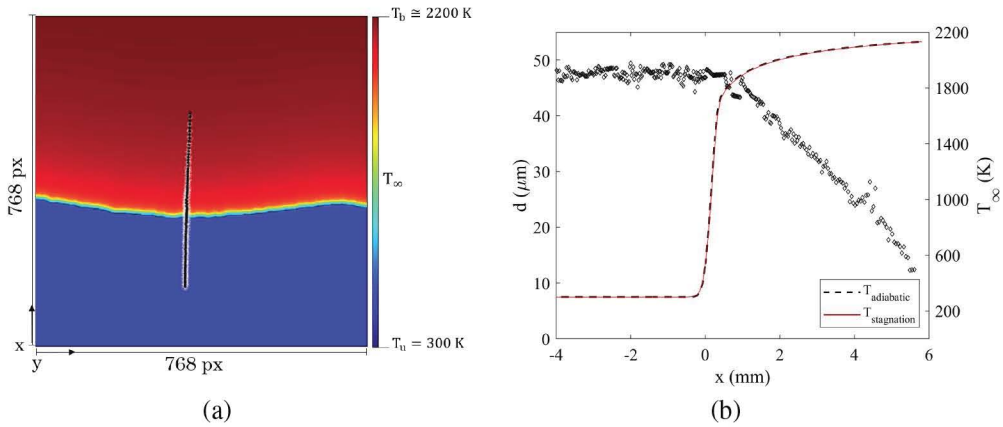

FIG. 4: (a) Fitted stagnation temperature profile and droplet trajectory (b) Variations in the droplet diameter (◇) and gas temperature for a stabilized stoichiometric CH_4/air flame and ethanol droplet (d_0 = 47 μm)

4. RESULTS AND DISCUSSION

4.1 Evaporation under pure N_2 ambient

The first comparison between experimental and numerical ethanol droplet evaporation rates is performed under stagnant N_2 ambient conditions. Saharin et al. studied the evaporation of isolated, anhydrous ethanol droplets (Saharin et al., 2012). The experiments were performed under N_2 ambient at varying temperatures between 373-673 K and the temporal evolution of the droplet diameter was recorded using a high-speed camera. The results are given in Fig. 5, with the numerical results for corresponding cases.

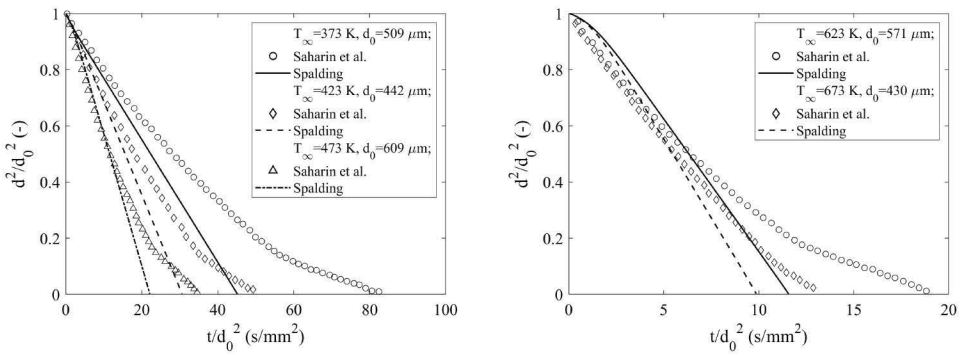

(a) (b)

FIG. 5: Comparison of ethanol droplet evaporation computations with the experiments of Saharin et al. (Saharin et al., 2012) and simulations via Spalding model under pure N_2 ambient at P=1 atm (a) low temperatures (b) high temperatures

Saharin et al. observed a deviation from the linear evaporation profile due to the condensation of water vapor on the droplet surface and the simultaneous evaporation of ethanol and water. The condensation effect is observed to be more important at lower ambient temperatures because of the high miscibility of ethanol to water. However, for high temperature cases, an almost linear behavior is observed for ethanol evaporation with a higher droplet lifetime than the one computed with the Spalding model. Due to the experimental technique used in the measurements, it is expected to observe a lower evaporation constant since the effects of heat conduction in the quartz fiber are limited; leading to the observation of higher evaporation times (Chauveau et al., 2019). For a stationary droplet, the numerical results are in a good agreement with the

experiments, especially at higher ambient temperatures.

4.2 Evaporation under flame conditions

Velocity measurements are performed for the droplet and unburnt gases via PTV and PIV, respectively. In Fig. 6, velocity profile of the ethanol droplet with an initial diameter of 47 μm, velocity profile of the unburnt gases of a stoichiometric flame measured up to the T=525 K isotherm as well as the computed profiles for different flame configurations are reported. For the stagnation flame configuration, velocity profile has a decreasing trend after the reaction zone due to the presence of a stagnation plate at which no-slip boundary condition is assumed to be complied.

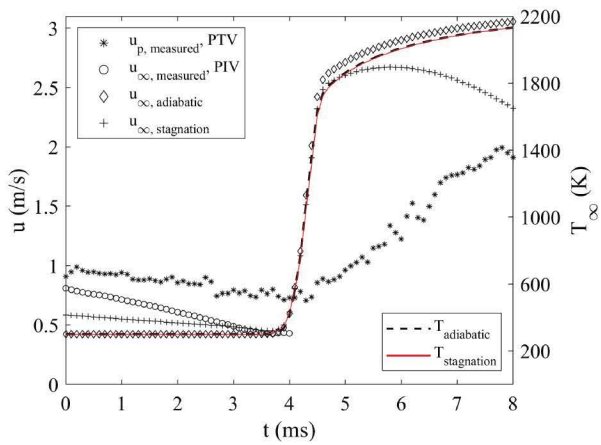

FIG. 6: Temporal evolution of the droplet velocity (PTV) and the measured (PIV) and computed gas velocities in stoichiometric condition (d_0=47 μm)

It is observed that there is a slight difference on the initial velocities of unburnt gases between PIV measurements and stagnation flame computations because of the fact that reported PIV data is calculated along the droplet path and the first detection of the droplet is achieved after a certain distance from the burner outlet, as can be seen in Fig. 4.a. Since the precision of the temperature profile is based on one isotherm (T=525 K), it is not accurate to report the exact location of the first droplet detection relative to the flame zone. It can still be concluded that PIV measurements provide reliable data, especially near to the flame zone.

It is known that the relative velocity between gas and liquid phases directly affects the evaporation rate due to the convection and its effects around a droplet along with Marangoni effect in the interface is critical in order to predict local/global evaporation rates correctly. From PTV and PIV measurements, the difference between droplet and gas velocities is computed to be small. Hence, the droplet is small enough to be carried by gas flow with a slight slip velocity. In the light of these information, convection around the droplet is found to be negligible under presented conditions. From Re_p computations, it is seen that through the entire domain, the value is below than 0.1 for all droplets demonstrating that convective effects from the surroundings are inconsequential for the droplet. This parameter naturally increases with the diameter of the droplet as well as with the increase in the speed of slip. However, the Reynolds numbers of droplets in burnt gases are always at the same order. Thus, the effect of forced convection on evaporation is negligible.

Temporal diameter evolution of the droplet having an initial diameter of 47 μm and evaporating under stoichiometric condition is reported in Fig. 7 below. Raw ILIDS measurements are given with diamond markers as well as the smoothed profile in order to observe the linearity during evaporation. For the simulations, the droplet diameter is kept constant at 50 μm which causes small differences with the experimental measurements because the latter contains high sampling of droplets between 20-70 μm. For experimental measurements, it should be noted that there might be slight changes in droplet measurement for different cases due to the difference in the initial position of the captured droplet and the droplet diameter measurement quality at certain frames. Since individual droplets are selected over all recorded experimental data, some droplets are initially tracked closer to the flame front. Therefore, the measured droplet trajectory is shorter for these droplets, making them difficult to track. Also, for the postprocessing of ILIDS data, Power Spectral Density (PSD) is estimated at two different orders at each frame in order to calculate the number of fringes. It is observed that for larger droplets, both methods give comparable data while for smaller droplets, higher order PSD captures the number of fringes in a more reliable way. This approach is generalized for all computations. Therefore, there may be some local deviations with a small error on the droplet diameter captured at certain positions,

especially close to the flame region where the change in diameter is expected to be higher in a shorter distance due to the steep temperature profile. Nevertheless, the accuracy of the diameter measurement can be assumed to be quite good at the flame zone, as reported in from Fig. 7.

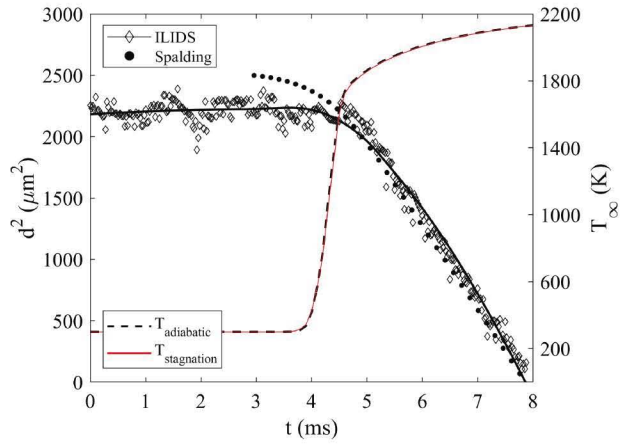

FIG. 7: Temporal evolution of the droplet diameter with ILIDS (d_0=47 μm, $T_{evap,average}$=2020.5±2.5 K) and Spalding model (d_0=50 μm, T_∞=2000 K) at stoichiometric conditions

The temperature of the ambient is defined as an average value for the experiments calculated from the beginning to the end of the evaporation curve. There is almost 3 K difference between stagnation and adiabatic profiles for the average value, whereas the difference becomes 8 K and 1 K at where the droplet starts to evaporate and its lifetime ends, respectively. In other words, for sufficiently small droplets which completely evaporate inside the reaction zone, it is slightly harder to define an exact ambient temperature. However, for the droplets spending most of their time in the burnt gases, evaporation temperature can be assumed as equal to the burnt gas temperature, regardless of exact position of the droplet with respect to the flame. Nevertheless, it should also be noted that the estimation of the temperature profile is directly linked to the stagnation plate temperature causing ±10 K temperature difference at the evaluated conditions.

In the initial stages of preheating, slightly different behavior is observed between data from experiments and simulations. This can be explained by the fact that for the simulations, the droplet meets immediately with the hot surroundings. However, experimentally, the droplet

spends enough time to adjust its velocity in the unburnt gases and gradually enters the reaction zone. In order to make a good comparison of droplet lifetime, the evaporation rate being the slope of d^2 vs. t from d^2 law given in Eq. (5), is computed over the diameter change interval is calculated after preheating zone. At the given condition in Fig. 7, K is reported as 0.67 and 0.55 mm^2/s from ILIDS measurement and Spalding computation, respectively. The difference between these values can be explained by two reasons. First of all, both the droplet and the surroundings are not stationary at experimental conditions which can cause convection and circulation effects. Secondly, the droplet is actually evaporating through a temperature field and the time spent at each isotherm is very small due to the steep behavior of the profile.

Fig. 8 shows the temporal evolution of the droplet temperature. Narasu et al. reported that the ambient composition has an influence on the droplet surface temperature causing the water condensation at lower ambient temperatures (Narasu et al., 2020). Considering the fact that one of the main products of the combustion is water, it is observed that the droplet temperature evolution trend is nearly the same under flame conditions and pure N_2 ambient. Therefore, it can be concluded that the condensation effect of water is negligible at high temperature conditions for ethanol droplets.

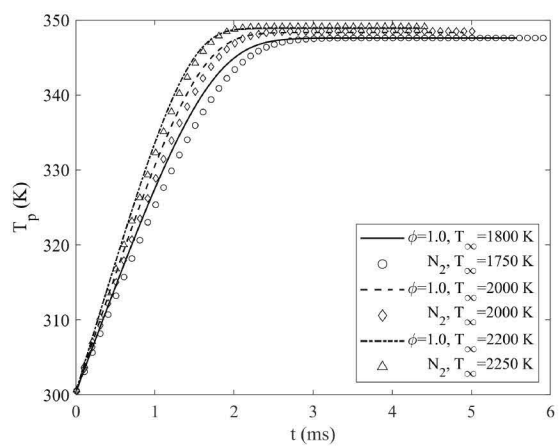

FIG. 8: Temporal evolution of the droplet temperatures at high temperature conditions

4.3 Rate of evaporation

In order to obtain droplet evaporation rate from d^2 law given in Eq. (5), slope of d^2 vs. t is computed over the diameter change interval. For each droplet, the mean temperature in this interval is recorded with the minimum and maximum values. Although the K values are in an acceptable range for all droplets evaporating at the same flame condition, there are slight changes due to the difference at the initial conditions of the captured droplet such as initial droplet diameter and droplet velocity.

Fig. 9 shows the dependency of the evaporation constant to the initial droplet size. The variability of the initial diameter provides a good database for the evaporation constant computed under the same conditions. However, for the sake of clarity to observe the effect of flame condition on evaporation, mean K values are computed and reported over all samples at each equivalence ratio with the error bars. For stoichiometric and rich flame conditions, large error bars are observed. However, it can be clearly seen that the majority of K values are located around 0.59 and 0.65 mm^2/s for ϕ=1.1 and 1.0, respectively. For lean flame conditions, it is seen that the variation range of K is even smaller. Therefore, it can be concluded that there is no major dependency of the evaporation constant to the initial size of the droplet at elevated conditions, as it is expected from d_2 law. Stokes number, defined as the ratio between the characteristic times of droplet and gas, is almost equal to 0.1 for all droplets. It implies that the velocity of the droplet quickly reaches to the gaseous phase velocity and the slip velocity between gas and droplet are comparably small for all conditions. Nevertheless, small deviations can be observed due to different experimental conditions and the initial condition of the droplet affecting the time spent at a certain temperature interval. It is also known that the vaporization rate of large droplets may be affected by drag forces although the computed Re_p numbers are quite small in an order of magnitude sense.

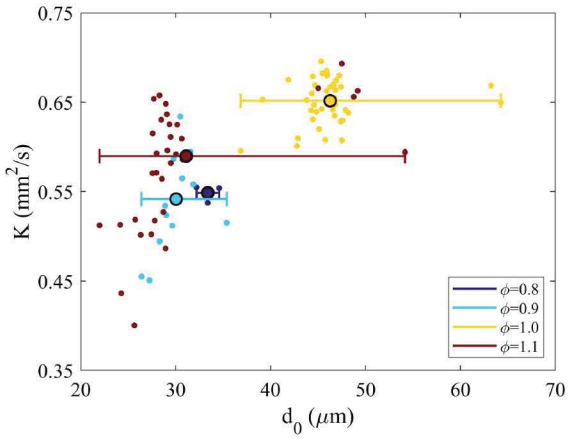

FIG. 9: Changes in ethanol evaporation constant with respect to the initial droplet diameter at different equivalence ratios

In order to compare the numerical results with flame experiments, burnt gas compositions are calculated in Cantera. COFFEE and San Diego mechanisms are used to differentiate the effect of species available in the surrounding gas since the latter contains ethanol in gas phase reactions. Evaporation computations are performed for each equivalence ratio at the ambient temperature varying between 1800-2200 K and at the burnt gas compositions, as well as at the flame compositions. It is observed that for lean and rich flame conditions, the evaporation constant is almost the same with the two mechanisms due to the fact that the compositions of major species, such as CH_4, CO_2, H_2O, are almost the same and the composition of ethanol at the ambient is nearly negligible. For stoichiometric flame condition, the difference between the evaporation constants at lower ambient temperature (1800-1900 K) is $\approx$0.02 mm^2/s which is decreasing towards higher temperatures. It is clearly seen that the ambient gas composition has no major effect on the evaporation under evaluated conditions.

It is observed in Fig. 9 that K values are varying between 0.6-0.7 mm^2/s for the stoichiometric flame while for ϕ=0.9 and 1.1, a wider range is observed. It should be noted that this is mostly due to the high sampling at these equivalence ratios and the differences on the initial conditions of droplets. As it is explained previously, the droplets are tracked initially at different locations since isolated droplets are selected from the whole experimental recording. Although the initial

location of each droplet is almost the same, its velocity may vary which affects directly the temperature exposure time at the flame zone, consequently, the evaporation constant. Therefore, instead of selecting some droplets, the mean values of K, mean interval temperature, minima and maxima are computed and reported in Fig. 10 over all samples at each equivalence ratio based on the stagnation flame temperature profile. For the Spalding model results at the burnt gas conditions, only one case is included for the sake of clarity since the computed evaporation constant is almost the same at different equivalence ratios with both kinetic mechanisms.

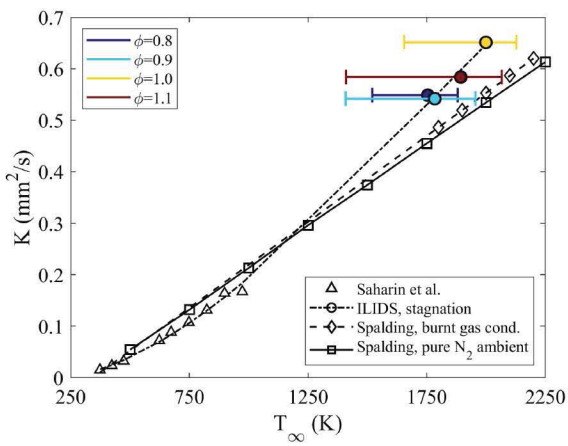

FIG. 10: Comparison of ethanol evaporation constant with respect to temperature

It is observed that the Spalding model overestimates the evaporation rate for low temperatures when it is compared with the experimental results of Saharin et al. However, for high temperatures and flame conditions, higher evaporation rates are measured experimentally. It should also be noted that Re_p numbers are computed for all cases as $\approx$0.1 in order of magnitude indicating that there is no major effect of relative velocity of the droplet.

The evaporation temperature is selected as the mean temperature in an interval where the droplet starts evaporating and its lifetime ends, since there is no way to measure the exact evaporation temperature of a moving droplet through a flame field. Still, maxima of the measured evaporation constants are very close to the numerical results. Although, there is a slight difference due to the different temperature profiles of adiabatic and stagnation flame configurations since the latter includes the heat loss effects to the stagnation plate. From the comparison of two

flame temperature profiles, it is observed that same K values yield lower mean interval temperatures for stagnation flames with a wider range from the minimum value. In other words, the droplet starts to evaporate at lower temperatures through the stagnation flame and the lifetime of the droplets ends at comparably similar temperatures for both flames. From these results, it can be interpreted that the heat losses has an impact on evaporation by lowering the ambient temperature which the droplet is exposed to while evaporating.

5. CONCLUSIONS

This paper describes the evaporation of a single ethanol droplet at flame conditions. Experiments are conducted in a stagnation flame burner configuration where the droplet is injected through a laminar, flat and stationary premixed CH_4/air flames at ϕ=0.8, 0.9, 1.0 and 1.1. Particle Reynolds number, Re_p is calculated based on PIV/PTV measurements as 10^{-1} indicating that the droplets can follow the gas flow with a relatively small slip velocity. This leads to the assumption that the convective effects around the droplet can be neglected. The diameter of the droplet is simultaneously measured via ILIDS at each 25 μs and the evaporation rate is calculated from the diameter change interval providing a database at elevated conditions for ethanol vaporization. The evaporation takes place at a very steep temperature profile while the major part is observed at the burnt gases based on the fitted temperature profiles computed from Cantera for 1D adiabatic freely propagating and stagnation flame configurations. Therefore, the vaporization temperature can be reported as burnt gas temperature, sensitive to heat exchange between the stagnation plate and flame whose effects are not introduced for adiabatic configuration. Hence, the heat losses to the stagnation plate have a slight effect on the evaporation rate of the droplet since it causes temperature changes. It is also observed that under the same ambient conditions, evaporation rate is not changing drastically depending on the initial droplet size for a range of 20-70 μm. Numerical computations are performed under pure N_2 ambient and burnt gas compositions for an isolated ethanol droplet. While pure N_2 ambient computations agree well with the literature at low temperatures, Spalding model underestimates the evaporation rate at higher temperatures. It is also concluded that ethanol droplet evaporation under the present conditions is not directly

affected by the changes in ambient gas composition at flame conditions.

ACKNOWLEDGMENTS

The authors acknowledge CNES for its financial support and CNRS CORIA for permitting the use of YALES2 code, special thanks to Dr. Vincent Moureau for his guidance. DK acknowledges the financial support of the French Embassy in Ankara for her joint PhD program between METU and the Université d'Orléans and TÜBİTAK BİDEB 2211-C scholarship programme.

REFERENCES

Abramzon, B. and Sirignano, W.A., Droplet vaporization model for spray combustion calculations, *International journal of heat and mass transfer*, vol. **32**, no. 9, pp. 1605–1618, 1989.

Al Qubeissi, M., Al-Esawi, N., Sazhin, S.S., and Ghaleeh, M., Ethanol/gasoline droplet heating and evaporation: Effects of fuel blends and ambient conditions, *Energy & Fuels*, vol. **32**, pp. 6498–6506, 2018.

Chauveau, C., Birouk, M., Halter, F., and Gokalp, I., An analysis of the droplet support fiber effect on the evaporation process, *International Journal of Heat and Mass Transfer*, vol. **128**, pp. 885–891, 2019.

Chen, G., Aggarwal, S., Jackson, T.A., and Switzer, G.L., Experimental study of pure and multicomponent fuel droplet evaporation in a heated air flow, *Atomization and Sprays*, vol. **7**, 1997.

Coffee, T.P., Kinetic mechanisms for premixed, laminar, steady state methane/air flames, *Combustion and Flame*, vol. **55**, pp. 161–170, 1984.

Driscoll, J.F., Turbulent premixed combustion: Flamelet structure and its effect on turbulent burning velocities, *Progress in Energy and Combustion Science*, vol. **34**, pp. 91–134, 2008.

Ghassemi, H., Baek, S.W., and Khan, Q.S., Experimental study on evaporation of kerosene droplets at elevated pressures and temperatures, *Combustion Science and Technology*, vol. **178**, pp. 1669–1684, 2006.

Gokalp, I., Chauveau, C., Berrekam, H., and Ramosarroyo, N., Vaporization of miscible binary fuel droplets under laminar and turbulent convective conditions, *Atomization and Sprays*, vol. **4**, pp. 661–676, 1994.

Goodwin, D.G., Speth, R.L., Moffat, H.K., and Weber, B.W., Cantera: An Object-oriented Software Toolkit for Chemical Kinetics, Thermodynamics, and Transport Processes, , 2018.

Hubbard, G.L., Denny, V.E., and Mills, A.F., Droplet evaporation: Effects of transients and variable properties, *International Journal of Heat and Mass Transfer*, vol. **18**, pp. 1003–1008, 1975.

Keller, P., Knorsch, T., Wensing, M., and Hasse, C., Experimental and numerical analysis of iso-octane/ethanol sprays under gasoline engine conditions, *International Journal of Heat and Mass Transfer*, vol. **84**, 2015.

Lawes, M., Lee, Y., and Marquez, N., Comparison of iso-octane burning rates between single-phase and two-phase combustion for small droplets, *Combustion and Flame*, vol. **144**, no. 3, pp. 513–525, 2006.

Maqua, C., Castanet, G., and Lemoine, F., Bicomponent droplets evaporation: Temperature measurements and modelling, *Fuel*, vol. **87**, pp. 2932–2942, 2008.

Mercier, X., Orain, M., and Grisch, F., Investigation of droplet combustion in strained counterflow diffusion flames using planar laser-induced fluorescence, *Applied Physics B*, vol. **88**, pp. 151–160, 2007.

Millán-Merino, A., Fernández-Tarrazo, E., and Sánchez-Sanz, M., Theoretical and numerical analysis of the evaporation of mono- and multicomponent single fuel droplets, *Journal of Fluid Mechanics*, vol. **910**, 2021.

Moureau, V., Domingo, P., and Vervisch, L., Design of a massively parallel CFD code for complex geometries, *Comptes Rendus Mécanique*, vol. **339**, pp. 141–148, 2011.

Muelas, , Carpio, J., Ballester, J., Sánchez, A.L., and Williams, F.A., Pyrolysis effects during high-temperature vaporization of alkane droplets, *Combustion and Flame*, vol. **217**, pp. 38–47, 2020.

Narasu, P., Boschmann, S., Pöschko, P., Zhao, F., and Gutheil, E., Modeling and simulation of single ethanol/water droplet evaporation in dry and humid air, *Combustion Science and Technology*, vol. **192**, pp. 1233–1252, 2020.

Nassouri, M., Chauveau, C., Halter, F., and Gökalp, I., Flame structure of ethanol-air premixed mixtures at high pressures in microgravity, *European Combustion Meeting (ECM2013)*, 2013.

Ni, Z., Hespel, C., Han, K., and Foucher, F., The non-ideal evaporation behaviors of ethanol/heptane droplets: Impact on diameter, temperature evolution and the light scattering by droplet at the rainbow angle, *International Journal of Heat and Mass Transfer*, vol. **164**, p. 120401, 2021.

Orain, M. and Hardalupas, Y., Droplet characteristics and local equivalence ratio of reacting mixture in spray counterflow flames, *Experimental Thermal and Fluid Science*, vol. **57**, pp. 261–274, 2014.

Peters, N., Laminar diffusion flamelet models in non-premixed turbulent combustion, *Progress in Energy*

and Combustion Science, vol. **10**, pp. 319–339, 1984, publisher: Pergamon.

Pinheiro, A.P., Vedovoto, J.M., Neto, A.d.S., and Wachem, B.G.M.v., Ethanol droplet evaporation: Effects of ambient temperature, pressure and fuel vapor concentration, *International Journal of Heat and Mass Transfer*, vol. **143**, p. 118472, 2019.

Renoux, G., Étude expérimentale de l'interaction goutte/flamme : propagation d'une flamme dans un aérosol en microgravité et passage d'une goutte à travers un front de flamme, PhD Thesis, Université d'Orléans, CNRS ICARE, 2020.

Renoux, G., Halter, F., and Chauveau, C., Experimental Study of The Morphology of Two-Phase Flame Instabilities in Microgravity, *Atomization and Sprays*, vol. **28**, pp. 915–929, 2018.

Saharin, S.B., Lefort, B., Morin, C., Chauveau, C., Moyne, L.L., and Kafafy, R., Vaporization Characteristics of Ethanol And 1-Propanol Droplets at High Temperatures, *Atomization and Sprays*, vol. **22**, 2012.

Spalding, D.B., Combustion of Liquid Fuels, *Nature*, vol. **165**, pp. 160–160, 1950.

Thielicke, W. and Stamhuis, E.J., PIVlab – Towards User-friendly, Affordable and Accurate Digital Particle Image Velocimetry in MATLAB, *Journal of Open Research Software*, vol. **2**, 2014.

Thiesset, F., Halter, F., Bariki, C., Lapeyre, C., Chauveau, C., Gökalp, I., Selle, L., and Poinsot, T., Isolating strain and curvature effects in premixed flame/vortex interactions, *Journal of Fluid Mechanics*, vol. **831**, pp. 618–654, 2017.

Thimothée, R., Chauveau, C., Halter, F., and Gökalp, I., Experimental investigation of the mechanisms of cellular instabilities developing on spherical two-phase flames, *Combustion Science and Technology*, vol. **188**, no. 11-12, pp. 2026–2043, 2016.

Thimothée, R., Chauveau, C., Halter, F., and Gökalp, I., Experimental investigation of the passage of fuel droplets through a spherical two-phase flame, *Proceedings of the Combustion Institute*, vol. **36**, pp. 2549–2557, 2017.

University of California San Diego, Mechanical and Aerospace Engineering-Combustion Research, Chemical-kinetic mechanisms for combustion applications v. 2016-12-14, , 2016.
URL `http://combustion.ucsd.edu`

Verdier, A., Marrero Santiago, J., Vandel, A., Godard, G., Cabot, G., and Renou, B., Local extinction mechanisms analysis of spray jet flame using high speed diagnostics, *Combustion and Flame*, vol. **193**,

pp. 440–452, 2018.

Verwey, C. and Birouk, M., Experimental investigation of the effect of natural convection on the evaporation characteristics of small fuel droplets at moderately elevated temperature and pressure, *International Journal of Heat and Mass Transfer*, vol. **118**, 2018.

Yozgatligil, A., Park, S.H., Choi, M.Y., Kazakov, A., and Dryer, F.L., Burning and sooting behavior of ethanol droplet combustion under microgravity conditions, *Combustion Science and Technology*, vol. **176**, pp. 1985–1999, 2004.